Precipitation of auroral protons in detached arcs

Thomas J. Immel, Stephen B. Mende, Harald U. Frey, Laura M. Peticolas, and Charles W. Carlson

Space Sciences Laboratory, University of California, Berkeley, USA

Jean-Claude Gérard and Benoit Hubert

L'Université de Liège, Belgium

Stephen A. Fuselier

Lockheed Martin Advanced Technology Center, Palo Alto, California, USA

James. L. Burch

Southwest Research Institute, San Antonio, Texas, USA

[1] Recent global-scale observations by the IMAGE-FUV instrument demonstrate the existence of regions of particle precipitation at sub-auroral latitudes on the dayside. The signature of this precipitation is seen infrequently, but when so, it is clear in all 3 channels of the FUV instrument. A conjugate hemisphere conjunction with the FAST satellite demonstrates the presence of precipitating protons and the notable absence of precipitating electrons in these arcs. With this knowledge, one can determine the mean energy and energy flux of the precipitating protons by intercomparison of the response in the three FUV channels. Assuming that the protons have a kappa energy distribution, the mean energy is found to be ~20 keV, with a peak in total energy flux of ~1 mW/m^2/sec, consistent with fits to the FAST ion measurements. These phenomena are observed mainly during times of high solar wind dynamic pressure and variable interplanetary magnetic field, and are associated with earlier nightside enhancements in the brightness and latitudinal extent of the proton aurora. INDEX TERMS: 2704 Magnetospheric Physics: Auroral phenomena (2407); 0310 Atmospheric Composition and Structure: Airglow and aurora; 2768 Magnetospheric Physics: Plasmasphere; 2778 Magnetospheric Physics: Ring current

1. Introduction

[2] Auroral precipitation away from the normal auroral oval has been observed in visible wavelengths in ISIS-2 observations [*Anger et al.*, 1979; *Moshupi et al.*, 1979]. These aurorae took the form of bands and diffuse arcs extending over several hours of local time in the dusk-evening sector. These studies characterized the precipitation as electron aurorae, from comparisons of the emissions of OI and N$_2^+$, and from some in-situ measurements of precipitating particles. The proton fluxes were found to be relatively inconsequential.

[3] New studies of this phenomenon are now possible using the spectrographic imaging component of the Far Ultraviolet Imager on the IMAGE satellite [*Burch*, 2000; *Mende et al.*, 2000]. The proton imaging channel of the instrument (SI-12) suppresses exospheric emissions of the HI 121.6-nm emission line at line- center, while allowing red-shifted emissions originating from the interaction of precipitating protons with the atmosphere. This is accompanied by simultaneous observations of the FUV auroral emissions of the

Lyman Birge Hopfield (LBH) bands of N$_2$ by the Wideband Imaging Camera (WIC) and OI at 135.6 nm in the second channel of the SI instrument. Recent validation work shows good comparisons between in-situ observations of auroral electrons and protons and the expected instrumental responses [*Hubert et al.*, 2001; *Gerard et al.*, 2001]. The study can now be extended to include precipitation over the entire dayside, and to account for proton effects.

2. FUV Imaging: Detached Proton Arcs

[4] Images from the FUV SI-12 camera were obtained from 1325 UT on January 23 (day 23), 2001 until the end of the day, during which IMAGE had a continuous view of the entire oval. Select images of the proton aurora are shown in original image coordinates in Figure 1 at 12 minute intervals, from 2102 UT to the end of the day. As the imager descended from apogee, the signature of subauroral precipitation became apparent in the afternoon sector beginning around 2100 UT, separate from higher latitude auroral precipitation, but basically still connected to the main oval at noon. The feature is very distinct at 2216 UT, which can be seen in the corresponding frame of Figure 1. Around 2300 UT, the dusk sector proton aurora brightened considerably, followed by a dramatic separation of the auroral arc, where the equatorward portion separated completely from the oval and propagated to 65° magnetic latitude, while the main oval receded several degrees towards the pole. The sun direction for these images is indicated with an arrow in the upper left hand panel. Magnetic latitude contours of 25, 50 and 75° are shown for reference.

[5] Observations of several of these bright signatures of proton precipitation, show that they are often centered over the afternoon sector of local time, where the strongest emissions are observed in the 1500–1700 MLT range. From these global images, one can also discern an apparent correspondence between the nightside proton auroral brightness and the appearance of dayside subauroral forms. At times 35–50 minutes prior to the two most pronounced subauroral proton signatures, there are clear signatures of the enhancement in the dusk- midnight proton auroral oval brightness and its latitudinal extent.

3. FAST Conjunction: In-situ and Remote Determination of Energetics

[6] FAST is a polar orbiting satellite dedicated to making high-time resolution measurements of particle precipitation and electric and magnetic fields in the auroral environment [*Carlson et al.*,
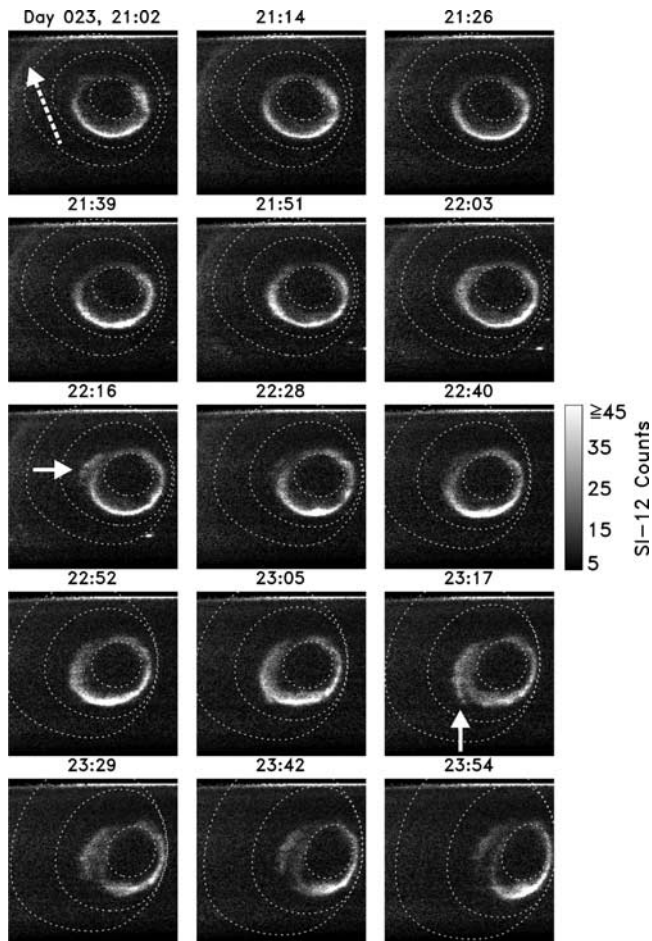
Figure 1. SI-12 images at 12 minute intervals beginning at 2102 UT on January 23, 2000. The direction to the sun is indicated in the first panel with a dashed arrow and geomagnetic latitudes of 25°, 50° and 75° are shown with dashed contours. Significant separation of an equatorward arc from the main oval is indicated with arrows at 2216 and 2317 UT.

of the total precipitating energy flux. Therefore, the peak proton energy flux that one would infer from the FAST observations of 0.2 mW/m²/sec is ~1.0 mW/m²/sec.

[8] It is clear from the FAST measurements of the electron energy spectrum (Figure 2a) and flux (Figure 2b) that electron precipitation which would cause emissions bright enough to be detected by WIC is not observed equatorward of −69.5° magnetic latitude. Therefore, the WIC and SI-12 imagers provide two independent measurements of the emissions produced by the subauroral proton precipitation. Using the work of *Hubert et al.* [2001], the LBH emissions created by a proton aurora can be compared with its Ly-α emissions to estimate the mean energy and total energy flux of the protons.

[9] Concurrent WIC and SI-12 images obtained at 2323 UT (25 minutes after the FAST pass) are compared at the time of maximum equatorward extent of the subauroral precipitation. These are mapped to geomagnetic coordinates centered at the north magnetic pole, and shown in Figure 3, along with line plots of the counting rates in each channel from the 1600 MLT meridian between 50 and 90 degrees magnetic latitude (indicated by a dashed line in the mapped images). In each image, dayglow emissions have been removed to reveal the underlying auroral emissions, using an empirically derived dayglow response model for each instrument [*Immel et al.*, 2000]. The dayglow correction
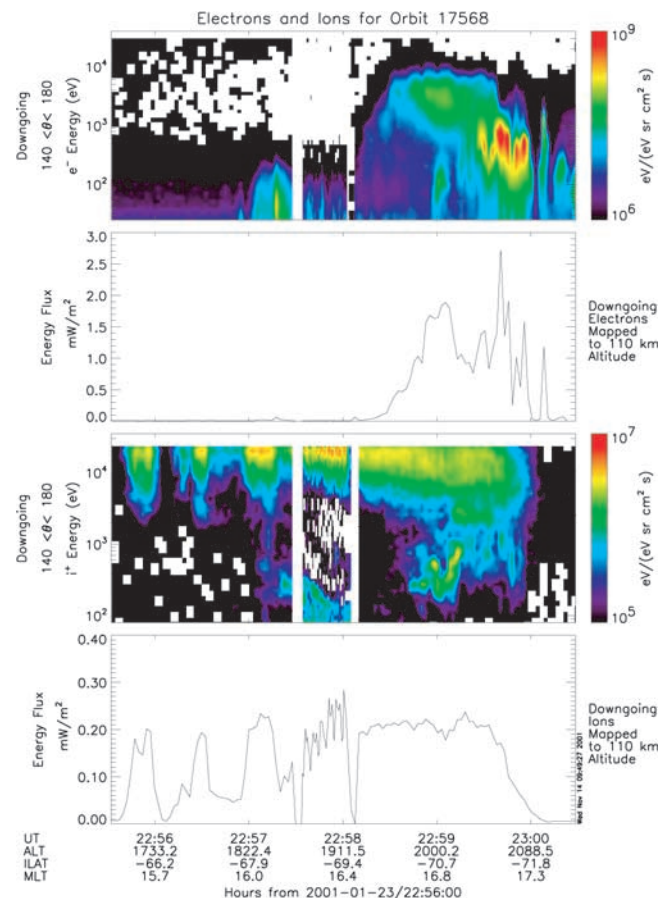
2001]. On day 23, at times between 2255 and 2300 UT, the satellite was in the 15−17 MLT sector, at magnetic latitudes between −65 and −72°. These are locations exactly conjugate to the subauroral enhancement observed in the northern hemisphere by IMAGE-FUV. Measurements of the electron and proton energy spectra from the FAST electrostatic analyzers are shown in Figure 2 as a function of UT, MLT, and magnetic latitude. The top panel shows the differential energy flux of electrons with pitch angles between 140 and 180° (Figure 2a), and with energies as high as 30 keV (the measurement limit of the analyzer). The next panel (Figure 2b) shows the integrated electron differential flux over these precipitating loss cone angles from the differential measurements. Like plots for the ion precipitation are shown in Figures 2c and 2d.

[7] The FAST data show a remarkably structured signature of significant proton precipitation, with three peaks in the energy flux at −65.5, −67.0, and −68.2° magnetic latitude. Assuming a Maxwellian distribution of energies, the mean energy per proton is found to be between 24 and 32 keV at these three locations. A fit with a kappa function, which was used in the IMAGE-FUV calibration and modeling, could result in a 10−20% increase in these mean energies, depending on the value of kappa. However, without measurements at energies >30 keV, such fits are not possible. Because of this limitation, the integrated precipitating energy flux observed by FAST is approximately a third to a fifth

Figure 2. Energy spectrograms of precipitating electron and proton energies a measured by the FAST electrostatic analyzer, conjugate to the IMAGE observations. The differential flux of electrons with pitch angles between 140° and 180° (precipitating), and the corresponding total energy flux are shown in Figures 2a and 2b, respectively. The same parameters from the ion measurements are shown in Figures 2c and 2d.

is small when compared to the counting rates from auroral emissions, particularly in the SI-12 channel, but is necessary to achieve the best determination of precipitating energy.

[10] The signature of the subauroral precipitation in the afternoon sector is clear in both SI-12 and WIC (Figures 3a and 3b, respectively), separate from the oval and extending from ∼1300 to 1800 MLT, with a peak in brightness near 1600 MLT at −64° magnetic latitude. Shown in the WIC counting rate plot are two dashed lines, which indicate the estimated contribution of the instrument response from proton produced secondary electrons [after *Hubert et al.*, 2001], assuming proton mean energies of 8 keV and 20 keV, represented by blue and red dashed traces, respectively. These show that proton precipitation of 20 keV would produce enough LBH emissions to account for the response of the WIC camera over most of the subauroral form. Indeed, the proton aurora must account for all of the emissions equatorward of −70°, as there is no significant electron precipitation at these latitudes. The peak of the proton energy flux inferred from the instrument response along this meridian is 1.2 mW/m^2/sec at −64°.

4. Discussion

[11] The appearance of subauroral proton precipitation in a specific local-time sector shows little similarity to any previously studied subauroral proton event, though the phenomenon has been noted on the nightside during substorm injections [*Sanchez et al.*, 1993]. The phenomenon compares well with the local time and latitude of similar auroral signatures observed by [*Moshupi*

Figure 3. Images from the FUV SI-12 and WIC imagers mapped to a projection of magnetic local time and latitude, with values along the 1600 MLT meridian shown below each map. Dayglow emissions are subtracted from each image such that the background count rate along the meridian in the line plots is ∼0. Included in the line plot for WIC are the calculated proton contribution to the WIC response, assuming 8 and 20 keV Maxwellian protons in blue and red, respectively.

et al., 1979], and the temporal duration of the signature at the dusk terminator is less than 110 minutes as noted in that study. However, contrary to the ISIS-2 observations, we find that protons are the primary component of the precipitating particle population. The N$_2$ LBH emissions that are usually associated with electron aurora are due, in this case, entirely to precipitating protons. These events are relatively rare, but often associated with a high dynamic pressure in the solar wind. Several instances where there is a clear signature which extends over more than 1 hour of local time are listed in Table 1.

[12] The mean energies observed by IMAGE and FAST are associated with protons which drift around the dusk sector of Earth after injection from the magnetotail [*DeForest and McIl-wain*, 1971]. These populations can either continue to drift as a part of the ring current, precipitate into the atmosphere, or exit the magnetosphere at some dayside local time sector, depending on the electric fields within the magnetosphere, the degree to which the solar wind has compressed the magnetopause, and the effectiveness of the initial injection in driving these protons to low L-shells. The morphology of the subauroral forms observed by IMAGE-FUV varies, but they often are connected to the auroral oval near noon, reaching lower latitudes further into the afternoon sector. Traced out along magnetic field lines to the magnetic equator, this corresponds approximately to drift paths of 24−32 keV protons which travel close to the Earth in the dusk sector and closer to the magnetopause at noon.

[13] The mechanism by which these protons are caused to precipitate must be explained, and there are several possibilities. An enhancement of the abundance of cold plasma in the ring current can cause the growth of the electromagnetic ion cyclotron (EMIC) instability, forcing ring current ions into the loss cone [*Brice and Lucas*, 1975, and references therein]. One might expect to observe this enhancement in plasmaspheric EUV images of HeII from IMAGE-EUV [*Sandel et al.*, 2001] in the form of a plasmaspheric bulge or a dense, sunward-directed tail. In the case presented here a tail was not observed, but the cold plasma densities required for instability growth (10−10^2 HeII/cc) are near the sensitivity threshold of the EUV instrument. Recent modeling of large magnetospheric storms shows that EMIC waves can contribute significantly to ion precipitation in the afternoon local time sector [*Jordanova et al.*, 2001].

[14] Increases in the number of protons in the loss cone can also be caused by a compression of the magnetopause, and the wave generation and ion heating which ensues [*Anderson and Hamilton*, 1993]. Subauroral proton precipitation has been observed by the SI-12 imager in conjunction with the arrival of shocked solar wind at Earth. However, with the slowly varying solar wind density and velocity observed during the time of this study (∼15 cm^{-3}, 475 km sec^{-1}), compression does not appear to be a factor. Possibly more significant is the steady northward turning of the Interplanetary magnetic field (IMF) between 1800 and 2200 UT B$_z$ from −8 to +4 nT), and the subsequent change in IMF B$_y$ between 2210 and 2330 UT (from −8 to +3 nT). The observed variation in IMF B$_z$ causes the auroral oval to retreat to higher latitudes, and may also provide the trigger for the nightside proton injections. A similar effect on the location of the oval caused by variations in IMF B$_y$ may also play a role, as discussed by *Burch et al.* [2002]. The favorable timing of the IMF rotations and proton injections may work to exaggerate the difference between the high-latitude and
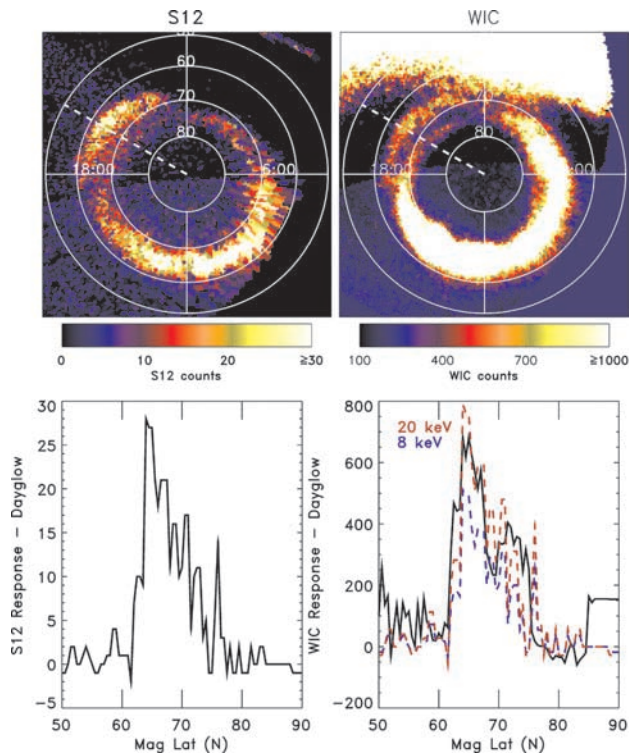
Table 1. Observations of Subauroral Proton Precipitation

Event	Date	Time (UT)
1	July 11, 2000	0750
2	November 10, 2000	0015
3	November 24, 2000	0945
4	January 23, 2001	2200
5	April 28, 2001	1110

subauroral emissions. Whether enhanced cold plasma densities are observed in the ring current during other periods of subauroral proton precipitation will be studied as part of a broad survey of these events [*Burch et al.*, 2002].

5. Conclusion

[15] These observations by IMAGE-FUV show a newly discovered phenomenon, which only now can be observed in a global sense. The SI-12 imager observed enhanced proton precipitation separate from the auroral oval over several hours of local time in the afternoon sector. The images also show significant enhancements in nightside proton precipitation preceding the dayside events by approximately 35–50 minutes. It is clear from the FAST data that the subauroral signature is purely the result of precipitating protons, which can be represented by a Maxwellian energy distribution with a 24–32 keV mean energy. After a substorm injection, protons with these energies will drift from near midnight to the afternoon sector in 45–70 minutes [*Roederer*, 1970]. The observations by FAST also show that the proton precipitation is highly structured, with three distinct proton 'arcs' appearing in the region. Any theory of the mechanism causing the proton precipitation must account for these periodic arcs.

[16] In summary, detached proton arcs appear after a favorable combination of events. These include a strong injection of protons from the magnetotail and large positive changes in IMF Bz. The relation to heightened solar wind densities is probably indirect, through the greater intensity of proton injections during these times. How the protons are caused to precipitate in regions separate from the auroral oval with the periodic arc-like structure observed by FAST, and how these observations relate to the detached electron aurorae observed with ISIS-2 are questions for future investigations.

References

Anderson, B. J., and D. C. Hamilton, Electromagnetic ion cyclotron waves stimulated by modest magnetospheric compressions, *J. Geophys. Res.*, *98*, 11,369–11,382, 1993.

Anger, C. D., M. C. Moshupi, D. D. Wallis, J. S. Murphree, L. H. Brace, and G. G. Shepherd, Detached auroral arcs in the trough region, *J. Geophys Res.*, *84*, 1333–1346, 1979.

Brice, N., and C. Lucas, Interaction between heavier ions and ring current protons, *J. Geophys. Res.*, *80*, 936–942, 1975.

Burch, J. L., Image mission overview, *Space Sci. Rev.*, *91*, 1–14, 2000.

Burch, J. L., W. S. Lewis, T. J. Immel, P. C. Anderson, H. U. Frey, S. A. Fuselier, J.-C. Gérard, S. B. Mende, D. G. Mitchell, and M. F. Thomsen, Interplanetary magnetic field control of afternoon-sector detached proton auroral arcs, *J. Geophys. Res.*, in press, 2002.

Carlson, C. W., J. P. McFadden, P. Turin, D.W. Curtis, and A. Magoncelli, The electron and ion plasma experiments for FAST, *Space Sci. Rev.*, *98*, 33–66, 2001.

DeForest, S. E., and C. E. McIlwain, Plasma clouds in the magnetosphere, *J. Geophys. Res.*, *76*, 3587–3611, 1971.

Gerard, J. C., B. Hubert, D. V. Bisikalo, V. I. Shematovich, H. U. Frey, S. B. Mende, and G. R. Gladstone, Observation of the proton aurora with IMAGE-FUV and simultaneous ion flux in situ measurements, *J. Geophys. Res.*, in press, 2001.

Hubert, B., J. C. Gerard, D. V. Bisikalo, and V. I. Shematovich, The role of proton precipitation in the excitation of the auroral FUV emissions, *J. Geophys. Res.*, *106*, 21,475– 21,494, 2001.

Immel, T. J., J. D. Craven, and A. C. Nicholas, An empirical model of the OI FUV dayglow from DE-1 images, *J. Atmos. and Solar-Terr. Phys.*, *62*, 47–64, 2000.

Jordanova, V. K., C. J. Farrugia, R. M. Thorne, G. V. Khazanov, G. D. Reeves, and M. F. Thomsen, Modeling ring current proton precipitation by electromagnetic ion cyclotron waves during the May 14–16, 1997, storm, *J. Geophys. Res.*, *106*, 7–22, 2001.

Mende, S. B., et al., Far ultraviolet imaging from the IMAGE spacecraft, 3. Spectral imaging of Lyman-α and OI 135.6 nm., *Space Sci. Rev.*, *91*, 287–318, 2000.

Moshupi, M. C., C. D. Anger, J. S. Murphree, D. D. Wallis, J. H. Whitteker, and L. H. Brace, Characteristics of trough region auroral patches and detached arcs observed by ISIS 2, *J. Geophys Res.*, *84*, 1333–1346, 1979.

Roederer, J. G., *Dynamics of Geomagnetically Trapped Radiation*, pp. 165, Springer-Verlag, New York, 1970.

Sanchez, E. R., B. H. Mauk, P. T. Newell, and C-.I. Meng, Low-altitude observation of the evolution of substorm injection boundary, *J. Geophys. Res.*, *98*, 5815–5838, 1993.

Sandel, B. R., R. A. King, W. T. Forrester, D. L. Gallagher, A. L. Broadfoot, and C. C. Curtis, Initial results from the IMAGE Extreme Ultraviolet Imager, *Geophys, Res. Lett.*, *28*, 1439–1442, 2001.

Stone, E. C., A. M. Frandsen, R. A. Mewaldt, E. R. Christian, D. Margolies, J. F. Ormes, and F. Snow, The Advanced Composition Explorer, *Space Sci. Rev.*, *86*, 1, 1998.

T. J. Immel, S. B. Mende, H. U. Frey, L. M. Peticolas, and C. W. Carlson, Space Sciences Laboratory, University of California, Berkeley, CA, 94720 USA. (immel@ssl.berkeley.edu)

J.-C. Gérard and B. Hubert, L'Université de Liège, Belgium.

S. A. Fuselier, Lockheed-Martin Advanced Technology Center, Palo Alto, California, USA.

J. L. Burch, Southwest Research Institute, San Antonio, Texas, USA.